SCIENCE CHINA
Earth Sciences

• RESEARCH PAPER •

January 2013 Vol.56 No.1: 153–164
doi: 10.1007/s11430-012-4435-y

Time constraints for the closing of the Paleo-Asian Ocean in the Northern Alxa Region: Evidence from Wuliji granites

ZHANG Wen, WU TaiRan*, FENG JiCheng, ZHENG RongGuo & HE YuanKai

Laboratory of Orogenic Belts and Crustal Evolution, Ministry of Education, School of Earth and Space Sciences, Peking University, Beijing 100871, China

Received April 17, 2011; accepted August 5, 2011; published online July 2, 2012

The Wuliji pluton in the Northern Alxa Region, Inner Mongolia, is the principal part of Shalazhashan Mountain. It belongs to the Zongnaishan-Shalazhashan Arc Zone, northwestern North China Plate, whose north is Engger Us Ophiolite Belt and south is Qagan Qulu Ophiolite Belt. The pluton was emplaced into Upper Carboniferous-Lower Permian Amushan Formation. According to the research about the original Carboniferous Amushan Formation, the lower and middle sections of the Carboniferous Amushan Formation consist of volcanic, clastic, and carbonate rocks, interpreted to represent the sedimentary association of a volcanic arc and back-arc basin; the upper section of the Amushan Formation is a molasse composed of silty shale, sandstone, gravel-bearing sandstone, and conglomerate. The Wuliji pluton consists mainly of biotite monzonitic granite, amphibole-bearing biotite monzonitic granite, and monzonitic granite. Geochemical analyses show that the pluton has both metaluminous and peraluminous characteristics, and on average has $SiO_2 > 70$ wt%, $Al_2O_3 > 14$ wt%, and high contents of Na_2O+K_2O (8.5 wt%), which define a calc-alkaline series. In addition, REE patterns show enrichment of LREE and weak negative Eu anomalies ($\delta_{Eu} = 0.3–1$). Altogether, the samples are depleted in Nb, Ta, Ti, P, Sr, and Ba, and enriched in Rb, Th, and K. These geochemical traits are interpreted to reflect an arc component. A secondary ion mass spectrometry (SIMS) U-Pb zircon age of the biotite monzonitic Wuliji pluton in the Northern Alxa Region, Inner Mongolia, is 250.8 ± 2.0 Ma (1σ). Samples have $\varepsilon_{Nd}(t)$ values between −0.1 and 1.3, which suggests that the granites were derived from mixing between the crust and mantle. Based on the SIMS age and geochemical characteristics, Wuliji granite is interpreted to be a post-collisional granite, the result of mantle-derived melt and assimilated juvenile arc crust. However, according to the newest international stratigraphic classification standard, the upper section of the Amushan Formation is Lower Permian in age, indicating that the back-arc basin had already closed in Early Permian. We conclude that the Paleo-Asian Ocean represented by the Engger Us Ophiolite Belt subducted southward in Late Carboniferous, at the same time that the trench-arc-basin system formed in the Northern Alxa Region. The Paleo-Asian Ocean was closed in Early Permian and the Northern Alxa Region entered a post-collisional period in the Late Permian, as indicated by the Wuliji granites. This suggests that the genesis of the Wuliji granites is consistent with the pluton emplacement at the upper crust, which occurred widely in the northern margin of the North China Plate in Late Carboniferous to Triassic.

Alxa, Engger Us, Qagan Qulu, SIMS, crust-mantle mixing, volcanic arc, post-collision

Citation: Zhang W, Wu T R, Feng J C, et al. Time constraints for the closing of the Paleo-Asian Ocean in the Northern Alxa Region: Evidence from Wuliji granites. Science China: Earth Sciences, 2013, 56: 153–164, doi: 10.1007/s11430-012-4435-y

The formation of the Central Asia Orogenic Belt (CAOB) is related to the evolution of the Paleo-Asian Ocean and its continental margins. However, the time of final closure of the Paleo-Asian Ocean is strongly debated. The final amalgamation time was regarded as either early Paleozoic [1–3], Devonian-Early Carboniferous [4–10] or Permian-Early or

*Corresponding author (email: twu@pku.edu.cn)

Middle Triassic [11–17]. The Alxa Region is located in the east of Inner Mongolia, China, belongs to the central part of CAOB, and connects the North China Plate, the Tarim Plate, and the Kazakhstan Plate. The geological and tectonic evolution of the area is so complicated that the relationship of the three plates and the Paleozoic tectonic evolution remain highly controversial. There are three important ophiolite belts or sutures in the Alxa Region (Figure 1(a)). From south to north, they are the Qagan Qulu Ophiolite Belt, the Engger Us Ophiolite Belt, and the Yagan Fault. The Engger Us Ophiolite Belt is regarded as the suture between the North China Plate and the Tarim Plate [11, 18–23]. The timing of obduction of the Qagan Qulu Ophiolite Belt and the Engger Us Ophiolite Belt has not been confirmed and, consequently, the timing of ocean closure represented by them remains controversial [11, 12, 18, 19, 24]. Shalazhashan Arc Zone lies between the Qagan Qulu Ophiolite Belt and the Engger Us Ophiolite Belt, and extends about 200 km from east to west with over 3000 km^2 of batholith. The formation of the Shalazhashan Arc Zone is related to the evolution of the southern continental margin of the Paleo-Asian Ocean. Determining the nature and the age of the Shalazhashan Arc Zone is significant, not only to the research of tectonic evolution of the Alxa Region, but also to the comparison between the east and west tectonic zones and to the speculation on the closure of the Paleo-Asian Ocean, the formational environment of the Qagan Qulu Ophiolite Belt, and the evolution of the Shalazhashan Arc Zone. The Wuliji pluton represents the Shalazhashan Arc Zone. The age obtained from U-Pb zircon dating, using secondary ion mass spectrometry (SIMS) and geochemical analysis, will help understand the genesis and the tectonic significance of Wuliji granites and constrain the tectonic evolution of the Wuliji area in the Late Paleozoic.

1 Geological setting and sample description

Six zones are delimited by the Yagan Fault, the Engger Us Ophiolite Belt, and the Qagan Qulu Ophiolite Belt in the Northern Alxa Region. From north to south they are the Yagan Upwarping Zone, the Zhusileng Early Paleozoic Passive Continental Margin, the Guaizihu Late Paleozoic Oceanic Basin, the Zongnaishan-Shalazhashan Arc, the Wuliji Back-arc basin, and the Yabulai-Bayinnuoergong Old Continent (Figure 1(a)). Together they comprise a

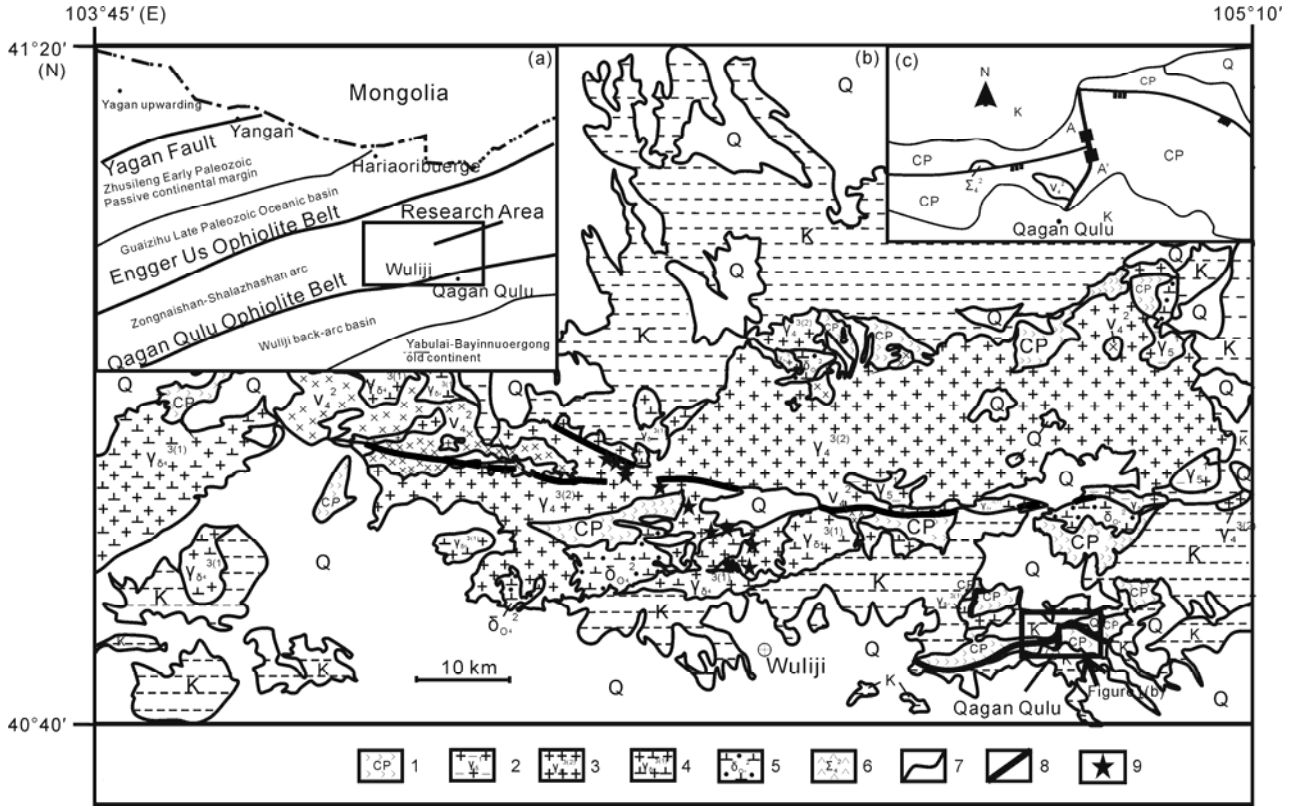

Figure 1 Regional tectonic sketch map of Northern Alxa Region (a), geological sketch map of Wuliji granites of Alxa Region (b) and the location of the profile of Qagan Qulu (c) (modified from footnotes 1–3)). 1. Upper Carbonferous-Lower Permian Amushan Formation; 2. Triassic red granite; 3. Permian granite; 4. Permian granodiorite; 5. Carbonferous quartz diorite; 6. Carbonferous pyroxene peridotite; 7. geological boundary; 8. fault; 9. sample.

1) Geological Survey Academy of Ningxia Hui Autonomous Region. Wuliji Regional Geological Survey Report (1∶200000), 1980

2) Geological Survey Academy of Ningxia Hui Autonomous Region. Shalataoerhan Regional Geological Survey Report (1∶200000), 1982

3) Geological Survey Academy of Ningxia Hui Autonomous Region. Yingen Regional Geological Survey Report (1∶200000), 1980

complete trench-arc-basin system of Late Paleozoic age. The Zongnaishan-Shalazhashan Arc Zone represented by Wuliji granites is the mature arc of this system, similar to today's Japan island arc [18, 25]. The Qagan Qulu Ophiolite Belt is regarded as the suture formed by the closure of back-arc basin during the Late Paleozoic [11, 12, 22, 23], and the Engger Us Ophiolite Belt is regarded as the suture representing the closure of the main ocean basin [11, 12, 18, 22, 23].

Igneous rocks of different ages are present in the Northern Alxa Region, and most of them are granites [11,18]. Many geochemical studies of the granites have been carried out [11, 18, 26–31], but few precise ages have been generated. To date, there are no well-constrained Permian-Triassic granites in the Northern Alxa Region, which would constrain the tectonic interpretation of the Paleozoic.

The Amushan Formation is the main Paleozoic unit in the Shalazhashan Zone, and thought to be of Upper Carboniferous age. Although it occurs non-uniformly in the area, a full composite section is represented. The lower section of the Amushan Formation consists of neritic intermediate-acid volcanic rocks, arkose, and shale, interpreted to represent volcanic rocks and clastic rocks. The middle section is composed mainly of neritic carbonate rocks. The upper section of the Amushan Formation is composed of coarse clastic sediments, such as feldspathic quartz sandstone and conglomerate. According to recent investigations [32–35], the upper section of the Amushan Formation previously regarded as Upper Carboniferous actually formed in the Zisongian Stage in the late Permian. From the profile of Qagan Qulu (Figures 1(c) and 2), a molasse composed of sandstone, gravel-bearing sandstone and conglomerate is found in the Amushan Formation, indicating that the back-arc basin represented by the Qagan Qulu Ophiolite Belt closed before the Early Permian.

The Wuliji pluton (Figure 1(b)), located about 8km north of Wuliji, Alxa Zuoqi, Inner Mongolia, is the principal part of Shalazhashan Mountain. The pluton represents a 1500 km^2 batholith emplaced into the Upper Carboniferous-Lower Permian Amushan Formation, and unconformably covered by Cretaceous strata. Its lithofacies are not well developed in this region, but medium-grained transitional facies and a few fine-grained marginal facies occur. The main rock type of the transitional facies is monzonitic granite, and the marginal facies consist of biotite-plagioclase granite and hybrid grandiorite. In particular, the Wuliji granite consists mainly of biotite monzonitic granite, amphibole-bearing biotite monzonitic granite, and monzonitic granite. All facies have massive structure without any layering. The model mineralogy is quartz (25%–45%), alkali feldspar (20%–35%) (mostly perthite and little K-feldspar), plagioclase (20%–45%), and mafic minerals (3%–15%) (mostly biotite and some hornblende). Zircon, sphene, apatite, and magnetite are the main accessory minerals.

2 SIMS U-Pb zircon geochronology

Sample W08-30 was processed for U-Pb analysis by conventional magnetic and density techniques to concentrate the non-magnetic, heavy minerals. Zircon crystals were mounted together with the zircon standard TEMORA in epoxy, which was then polished to section the crystals for analysis. All zircon grains were documented with transmitted and reflected light micrographs as well as cathodoluminescence (CL) images to reveal their internal structures. The mount was vacuum-coated with high-purity gold. U, Th, and Pb were measured using the Cameca IMS-1280 SIMS

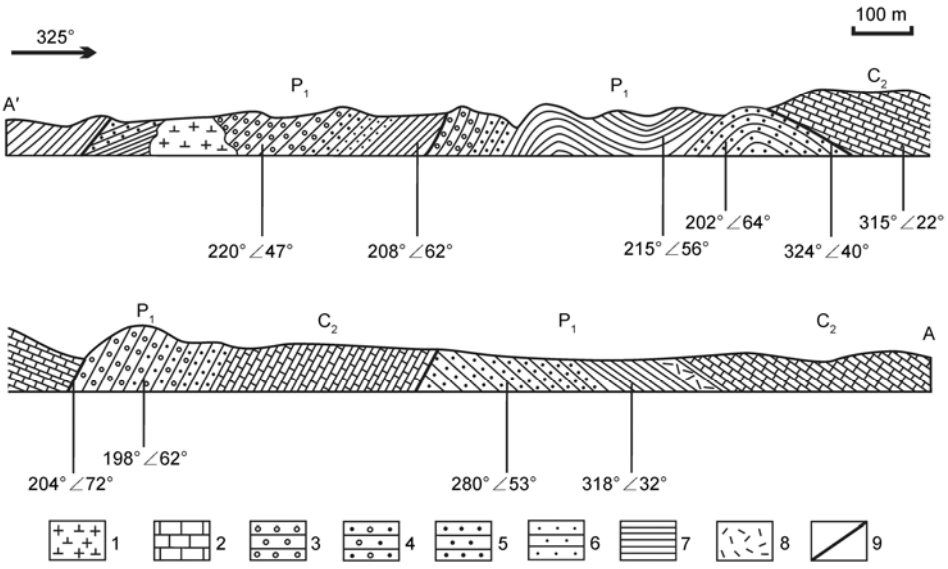

Figure 2 The profile of Qagan Qulu. 1. Granodiorite; 2. limestone; 3. conglomerate; 4. gravel-bearing sandstone; 5. sandstone; 6. siltstone; 7. shale; 8. rhyolite; 9. fault.

at the Institute of Geology and Geophysics, Chinese Academy of Sciences. Analytical procedures were the same as those described by Li et al. [36]. The ratio of the number of standard zircon grains to analyzed zircon grains was 1:3 during the test. Calibration of U-Th-Pb isotopic ratios was relative to the standard zircon TEMORA (417 Ma) [37], and U content was relative to the standard zircon 91500 (81 ppm) [38]. A long-term uncertainty of 1.5% (1 RSD) for $^{206}Pb/^{238}U$ measurements of the standard zircon grains was propagated to the unknowns [39], even though the measured $^{206}Pb/^{238}U$ error in a specific session was generally around 1% (1 RSD) or less. Measured compositions were corrected for common Pb using non-radiogenic ^{204}Pb. The content of common Pb was very low, which was largely derived from laboratory contamination introduced during sample preparation. An average present-day crustal composition was used for the common Pb [40]. Data reduction was carried out using the Isoplot 3.0 program [41]. The results are shown in Table 1. Uncertainties of individual analyses are reported at the 1σ level.

Fifteen analyses of 15 zircon grains were done (Figure 3). There are inherited cores in grains 7 and 9, but analysis 7 is located on oscillatory zoning and analysis 9 on an inherited core. Except for these analyses, all others represent idio-

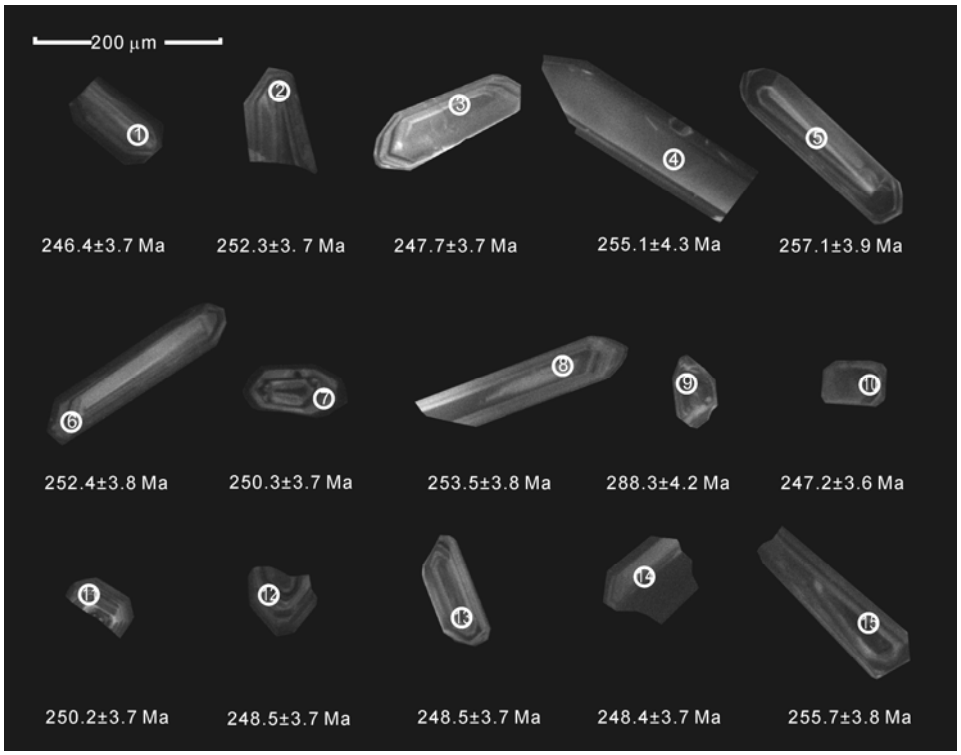

Figure 3 Cathodoluminescence (CL) images of zircon grains from the Wuliji pluton.

Table 1 Zircon SIMS U-Pb isotopic data of W08-30

Analysis No.	$^{232}Th/^{238}U$	$^{207}Pb/^{235}U$	$\pm1\sigma$ (%)	$^{206}Pb/^{238}U$	$\pm1\sigma$ (%)	$^{207}Pb/^{235}U$ age (Ma)	$\pm1\sigma$	$^{206}Pb/^{238}U$ age (Ma)	$\pm1\sigma$	Degree of concordance
W08-30@1	0.63	0.2857	3.4	0.0390	1.5	255.1	7.7	246.4	3.7	103.5
W08-30@2	0.54	0.2813	2.5	0.0399	1.5	251.7	5.5	252.3	3.7	99.8
W08-30@3	0.60	0.2792	2.7	0.0392	1.5	250.0	5.9	247.7	3.7	100.9
W08-30@4	0.41	0.2813	2.3	0.0404	1.7	251.7	5.1	255.1	4.3	98.7
W08-30@5	1.02	0.2825	2.6	0.0407	1.5	252.7	5.7	257.1	3.9	98.3
W08-30@6	0.61	0.2611	3.6	0.0399	1.5	235.6	7.5	252.4	3.8	93.3
W08-30@7	0.91	0.2747	2.6	0.0396	1.5	246.5	5.6	250.3	3.7	98.5
W08-30@8	0.60	0.2629	5.8	0.0401	1.5	237.0	12.2	253.5	3.8	93.5
W08-30@9	0.49	0.3233	2.8	0.0457	1.5	284.4	7.0	288.3	4.2	98.6
W08-30@10	0.88	0.2769	2.6	0.0391	1.5	248.2	5.7	247.2	3.6	100.4
W08-30@11	0.85	0.2787	2.6	0.0396	1.5	249.6	5.7	250.2	3.7	99.8
W08-30@12	0.64	0.2777	2.8	0.0393	1.5	248.8	6.1	248.5	3.7	100.1
W08-30@13	0.76	0.2674	3.5	0.0393	1.5	240.6	7.5	248.5	3.7	96.8
W08-30@14	0.79	0.2753	2.2	0.0393	1.5	247.0	4.9	248.4	3.7	99.4
W08-30@15	1.20	0.2829	2.0	0.0405	1.5	252.9	4.6	255.7	3.8	98.9

morphic grains with oscillatory zoning, interpreted as classic magmatic zircon grains. These analyses represent both rims and cores, but no old zircon grains or inherited cores were found. All analyses have high Th/U ratios between 0.410 and 1.201, which are characteristic of magmatic zircon [42, 43]. Integrating the shape, textures and high Th/U of the zircon grains, we conclude that most of the zircon grains are magmatic. All ages are concordant (The degree of concordance is 93.3–103.5 using the calculation $100\times^{207}Pb/^{235}U$ age/$^{206}Pb/^{238}U$ age). The older age of analysis 9 (288.6±4.3 Ma) excluded, weighted mean of $^{206}Pb/^{238}U$ of these fourteen analyses yields a concordia age of 250.8±2.0 Ma (MSWD=0.81) (Figure 4) and is interpreted as the crystallization age of sample W08-30. The zircon grain with an age of 288.6±4.3 Ma is interpreted as a xenocryst.

3 Geochemistry

3.1 Major elements

Major element analyses of the Wuliji granite are given in Table 2. The SiO_2 contents of the granites range from 68.83 wt%–74.44 wt%, and Al_2O_3 from 13.14 wt%–15.10 wt%. All of the rocks are metaluminous and peraluminous, with A/CNK ratios from 0.83 to 1.02 (Figure 5). The total alkali content (Na_2O+K_2O) is 8.51 wt% on average, and most samples contain more Na_2O than K_2O (Na_2O=4.16%–6.69%, K_2O=2.67%–5.22%). The samples are subalkaline with NK/A from 0.70 to 0.94 (Figure 6), and define to moderate to high potassium calc-alkaline suite (Figure 7). Rittmann indices ($\sigma=(Na_2O+K_2O)^2/(SiO_2-43)$) are from 2.02 to 3.18. In addition, P_2O_5 contents range from 0.01 wt%–0.13 wt%, TiO_2 from 0.09 wt%–0.63 wt%, TFe_2O_3 from 0.28 wt%–3.14 wt%, CaO from 0.56 wt%–3.06 wt%, and MgO from 0.01 wt% to 2.10 wt%. Bivariate element plots show that SiO_2 varies inversely with Al_2O_3, CaO, TiO_2, TFe_2O_3, and MgO, but lacks a systematic correlation with total alkalis (Figure 8). Geochemically, the rocks represent calc-alkaline series.

3.2 REE and trace elements

Total REE contents of Wuliji granites range from 56.73 to 100.75 ppm (Table 2). Chondrite-normalized REE patterns (Figure 9) show enrichment of LREE with $(La/Yb)_N$ values

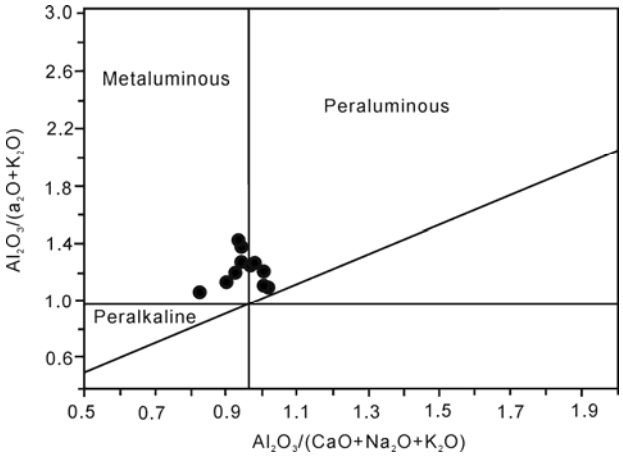

Figure 5 Shand's Index diagram of Wuliji granites [44].

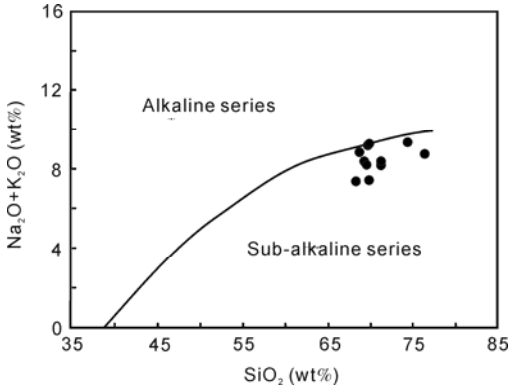

Figure 6 Alkalinity ratio versus SiO_2 diagram [45].

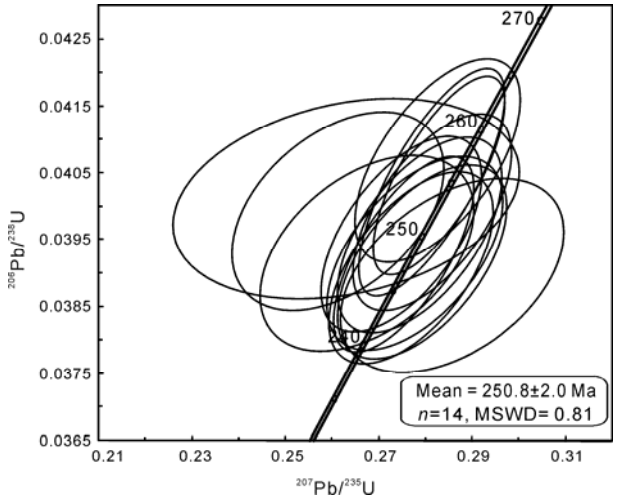

Figure 4 U-Pb concordia plot for Wuliji granite.

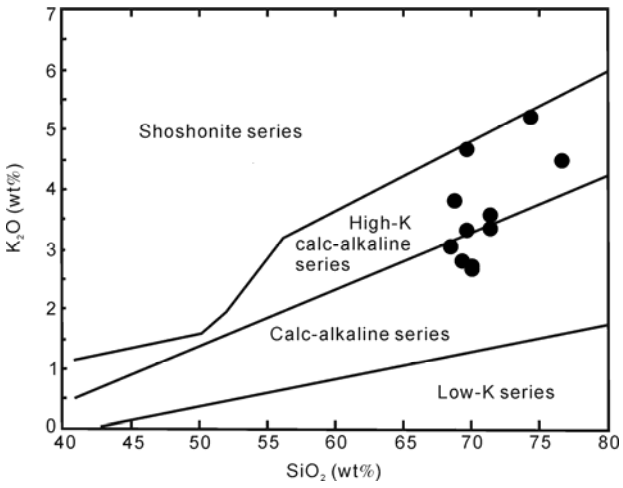

Figure 7 K_2O vs SiO_2 diagram of Wuliji granites [46].

Table 2 Chemical composition of Wuliji granites[a)]

Sample No.	W08-29	W08-41	W08-52	W08-65	W08-70	W08-30	W08-22	W08-34	W08-45	W08-63	W08-69
SiO_2	74.44	68.83	69.35	69.66	69.73	76.51	69.92	68.35	71.27	69.90	71.28
Al_2O_3	0.09	0.30	0.24	0.28	0.27	0.11	0.53	0.63	0.35	0.33	0.34
TFe_2O_3	13.76	15.10	14.85	15.00	14.28	13.14	14.67	14.85	14.56	14.84	14.65
CaO	0.28	1.83	1.70	1.58	1.66	0.34	2.62	3.14	1.89	1.52	1.76
MgO	0.04	0.04	0.03	0.03	0.03	0.03	0.04	0.05	0.04	0.02	0.03
K_2O	0.84	2.10	1.78	1.95	1.69	0.01	1.31	1.80	0.91	0.72	0.76
Na_2O	0.56	1.40	2.03	2.29	1.81	0.67	2.75	3.06	1.87	2.27	1.93
MnO	4.16	5.05	5.65	4.93	4.54	4.28	4.71	4.32	4.81	6.69	4.77
TiO_2	5.22	3.83	2.81	3.34	4.68	4.46	2.67	3.04	3.34	2.70	3.57
P_2O_5	0.01	0.10	0.07	0.08	0.08	0.01	0.11	0.13	0.09	0.09	0.08
LOI	0.55	1.31	1.41	0.77	1.12	0.39	0.58	0.51	0.76	0.81	0.74
Total	99.96	99.90	99.91	99.91	99.91	99.96	99.90	99.90	99.89	99.88	99.90
σ	2.80	3.06	2.72	2.56	3.18	2.28	2.02	2.14	2.35	3.28	2.46
AR	3.78	3.33	3.01	2.83	3.59	4.26	2.47	2.40	2.97	3.43	3.02
NK/A	0.91	0.82	0.83	0.78	0.88	0.90	0.73	0.70	0.79	0.94	0.80
A/NCK	1.02	1.01	0.93	0.94	0.90	1.00	0.94	0.93	0.97	0.82	0.96
Rb	249.0	117.5	64.8	109.0	162.3						
Ba	171.4	510.2	408.5	381.9	434.5						
Th	20.67	13.95	5.59	14.17	13.24						
U	3.74	2.60	1.20	2.17	1.88						
Nb	12.19	8.25	4.62	5.59	6.66						
Ta	1.27	0.97	0.44	0.51	0.71						
Pb	38.35	23.92	14.84	22.40	33.11						
Sr	128.5	339.7	375.2	386.2	253.9						
Zr	79.6	170.4	96.5	161.5	137.0						
Hf	4.12	6.20	3.50	5.75	5.13						
Li	55.34	29.86	53.27	31.01	36.46						
Be	3.70	2.95	1.36	2.10	2.52						
Sc	3.28	3.77	3.77	4.39	3.71						
V	9.34	34.86	23.15	36.60	30.83						
Co	5.16	8.18	5.77	7.84	5.98						
Ga	17.57	18.77	17.16	20.21	18.73						
Cs	171.4	5.9	3.7	5.1	7.5						
La	12.82	21.24	11.08	12.03	17.95						
Ce	28.00	44.18	22.96	30.60	38.54						
Pr	3.30	4.62	2.83	2.89	3.98						
Nd	12.32	17.13	10.73	10.86	14.51						
Sm	2.76	3.21	2.01	1.97	2.50						
Eu	0.25	0.86	0.65	0.60	0.60						
Gd	2.90	3.14	2.03	1.88	2.37						
Tb	0.49	0.44	0.28	0.23	0.29						
Dy	3.05	2.39	1.59	1.24	1.53						
Ho	0.62	0.46	0.31	0.23	0.28						
Er	1.96	1.33	0.94	0.67	0.83						
Tm	0.32	0.20	0.14	0.10	0.13						
Yb	2.28	1.36	1.02	0.72	0.90						
Lu	0.34	0.20	0.16	0.11	0.14						
Y	19.56	12.93	8.48	6.16	7.95						
REE	71.4	100.8	56.7	64.1	84.6						
LREE	59.5	91.2	50.3	59.0	78.1						
HREE	12.0	9.5	6.5	5.2	6.5						
LREE/HREE	5.0	9.6	7.8	11.4	12.1						
$(La/Yb)_N$	3.64	10.11	7.02	10.78	12.90						
δ_{Eu}	0.27	0.83	1.00	0.97	0.75						
10000×Ga/Al	2.41	2.35	2.18	2.55	2.48						

a) Geochemical analyses were performed at the School of Earth and Space Sciences, Peking University. Major elements (%) were analyzed by ADVANT`XP+XRF from Thermo Electron Corporation, America, and rare and trace elements (ppm) were analyzed by Agilent 7500Ce ICP-MS. $AR=(Al_2O_3+CaO+Na_2O+K_2O)/(Al_2O_3+CaO-Na_2O-K_2O)$, $\delta_{Eu}=Eu_N/\sqrt{Sm_N\times Gd_N}$.

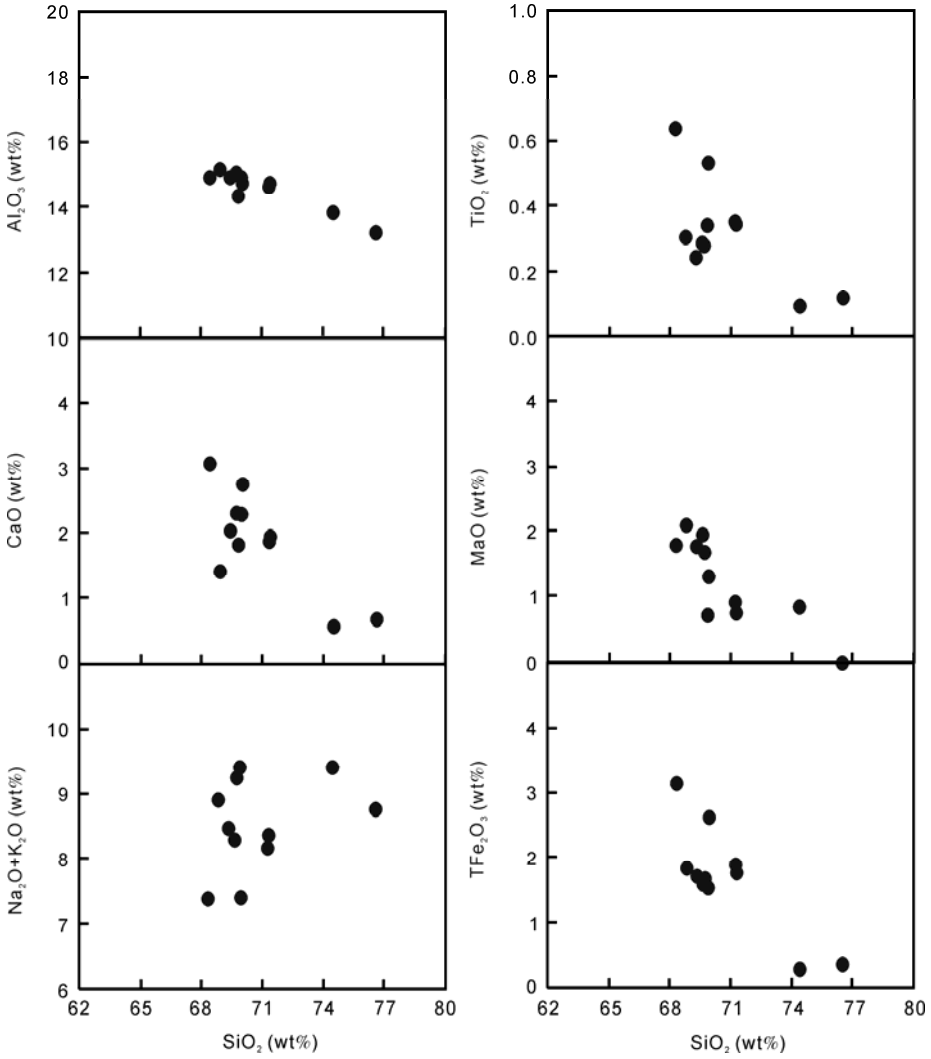

Figure 8 Bivariate element plots.

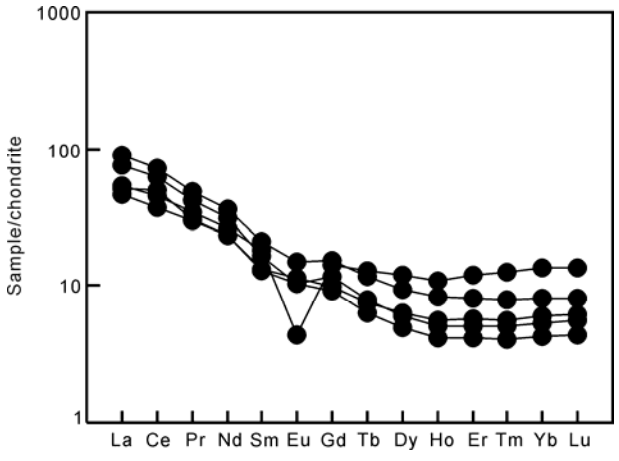

Figure 9 Chondrite-normalized REE patterns (normalized values after ref. [47]).

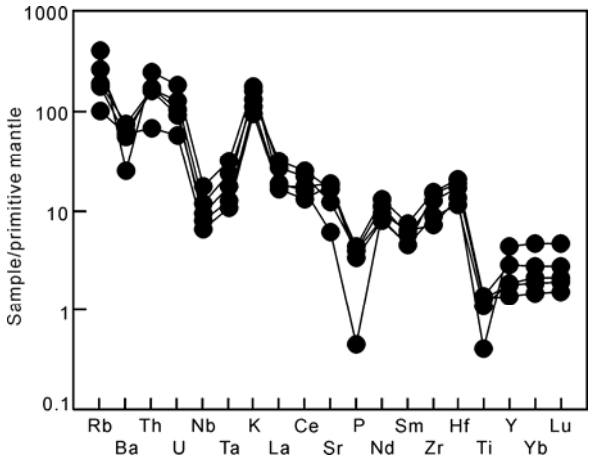

Figure 10 Primitive mantle-normalized trace elements patterns (normalized values after ref. [47]).

of 3.64–12.90 and weak negative Eu anomalies (δ_{Eu} = 0.3–1). Compared to other samples, W08-29 has a greater negative Eu anomaly and lower SiO_2, and lacks anorthite.

All samples have similar, roughly parallel chondrite-

normalized REE patterns and primitive mantle-normalized trace elements patterns (Figure 10), indicating they could be from the same source. The samples are depleted in Nb, Ta, Ti, P, Sr, and Ba, and enriched in Rb, Th, and K. In Sr vs. Yb plot [48, 49], all samples fall in low-Sr and low-Yb type (figure omitted). All samples represent typical volcanic arc granites (Figure 11). Over all, these geochemical traits are interpreted as reflecting an arc component.

4 Nd and Sr isotopic analysis

Analyses for Sr and Nd isotopes and Sm, Nd, Rb, and Sr contents were performed at the Institute of Geology, Chinese Academy of Geological Sciences (CAGS), using the Solid Isotope Mass Spectrometer MAT-262 from German Finnigan Corporation. Analytical procedures were described in detail by Yang et al. [52]. During analysis, the NBS-987 standard yielded an average value of $^{87}Sr/^{86}Sr=0.710274\pm11$ (2σ) and the JMC standard yielded an average value of $^{143}Nd/^{144}Nd=0.512096\pm12$ (2σ). Mass fractionation of Sr and Nd isotopes were corrected by $^{86}Sr/^{88}Sr = 0.1194$ and $^{146}Nd/^{144}Nd = 0.7219$. In the analyses, the backgrounds of Rb-Sr and Sm-Nd were 100–300 and 50–100 pg, respectively. All isotopic results are summarized in Table 3.

From Table 3, Dongqiyishan granites have lower $(^{87}Sr/^{86}Sr)_i$ values than that of depleted mantle (0.7023), which is impossible for granites. So we do not discuss Rb and Sr isotopes in this paper. The Nd model ages have been calculated as $f_{Sm/Nd}$ ranges from −0.2 to −0.6 [53]. Wuliji granites define a field between DM and Paleoproterozoic-Mesoproterozoic crust in the diagram $\varepsilon_{Nd}(t)$ vs. intrusive age (Figure 12), indicating a mix of crustal and mantle-derived magma. In the diagram $\varepsilon_{Nd}(t)$ vs. T_{DM} (Figure 12),

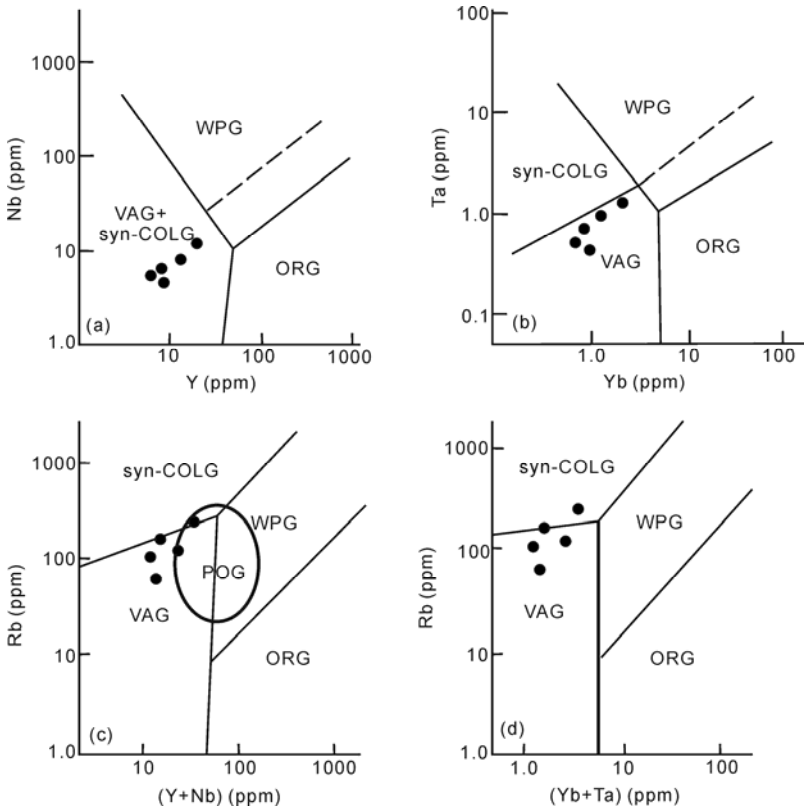

Figure 11 Trace element discrimination diagrams for the tectonic interpretation of granites [50, 51]. WPG-within plate granites; syn-COLG-syn-collision granites; VAG-volcanic arc granites; ORG-ocean ridge granites; POG-post-collision granites.

Table 3 Isotopic analyses for Sr and Nd of Wuliji Granites[a)]

Sample No.	$^{87}Rb/^{86}Sr$	$^{87}Sr/^{86}Sr$ ($\pm2\sigma$)	$(^{87}Sr/^{86}Sr)_i$	$^{147}Sm/^{144}Nd$	$^{143}Nd/^{144}Nd$ ($\pm2\sigma$)	$\varepsilon_{Nd}(0)$	$\varepsilon_{Nd}(t)$	$f_{Sm/Nd}$	t_{DM} (Ga)
W08-29	13.50	0.749624±13	0.70151	0.1344	0.512602±10	–0.70	+1.3	–0.32	1.05
W08-30	15.72	0.755908±15	0.69987	0.1185	0.512541±11	–1.89	+0.6	–0.40	0.97
W08-41	1.074	0.709081±14	0.70525	0.1151	0.512498±9	–2.72	–0.1	–0.42	1.01

a) $\varepsilon_{Nd} = [(^{143}Nd/^{144}Nd)_s/(^{143}Nd/^{144}Nd)_{CHUR}-1]\times10000$, $f_{Sm/Nd} = ((^{147}Sm/^{144}Nd)_s/(^{147}Sm/^{144}Nd)_{CHUR}-1)$; s=sample, $(^{143}Nd/^{144}Nd)_{CHUR} = 0.512638$, $(^{147}Sm/^{144}Nd)_{CHUR} = 0.1967$; Nd model ages: $t_{DM} = 1/\lambda\cdot\ln[1+((^{143}Nd/^{144}Nd)_s-0.51315)/((^{147}Sm/^{144}Nd)-0.2137)]$.

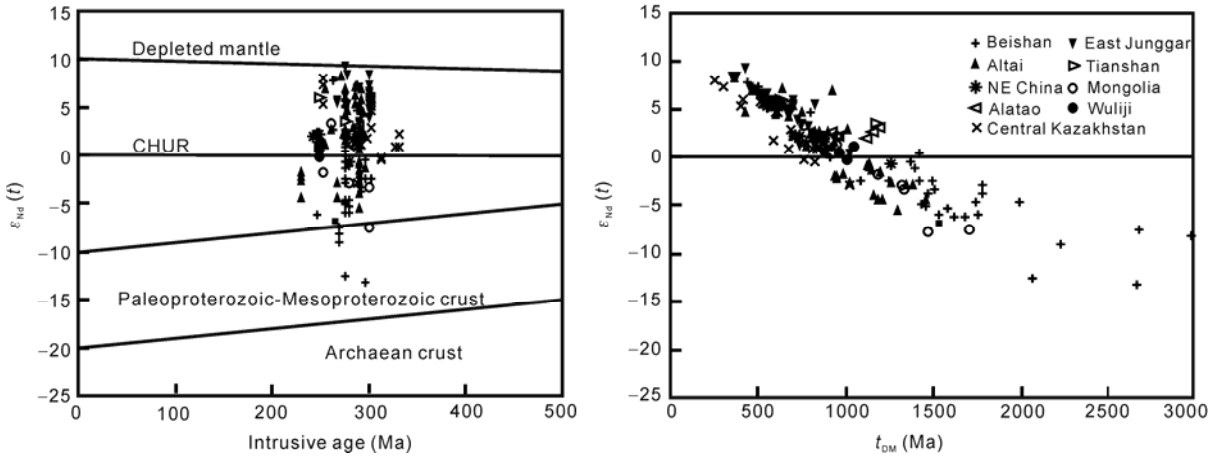

Figure 12 $\varepsilon_{Nd}(t)$ of Wuliji granites. Data of Beishan Mountain from refs. [54–56], East Junggar from refs. [57–60], Altai form refs. [57, 61–64], Tianshan Mountain from ref. [65], Northeast China from refs. [66,67], Alatao Mountain from ref. [68], Mongolia from refs. [69–70], Central Kazakhstan from ref. [71] and Wuliji from this study. Symbols are the same in both figures.

Wuliji samples are consistent with 230–300 Ma CAOB granitoids. In addition, $\varepsilon_{Nd}(t)$ is near 0. All these results suggest that a mantle component plays an important part in the genesis of Wuliji granites.

5 Genesis of Wuliji granites and their tectonic settings

Some geochemical traits of Wuliji granites are interpreted as reflecting an arc component. However, SiO_2 contents >70% on average, Al_2O_3 >14%, and A/NCK >1 imply the rocks are metaluminous and peraluminous. Negative Eu anomalies probably are related to residual plagioclase in the source. The depletion of Nb reflects the fact that the source of granites has a continental characteristic [72]. Zhang et al. [48, 49, 73] regard low-Sr and low-Yb type granites as likely to have formed under moderate pressure. In the diagram R1-R2 (Figure 13), most samples fall into the late-orogenic area. In addition, all samples show the similar, roughly parallel ocean ridge granite-normalized geochemical patterns representative of post-collision granites (Figure 14).

According to sedimentary investigation of the study of Amushan Formation, the lower and middle sections consist of volcanic rock, clastic, and carbonate rocks, interpreted as representing a sedimentary association of volcanic arc and back-arc basin, which is in agreement with the arc-related geochemical traits of Wuliji granites. This implies that the Paleo-Asian Ocean represented by the Engger Us Ophiolite Belt subducted southward in Late Carboniferous, when the trench-arc-basin system formed in the Northern Alxa Region. The upper section of the Amushan Formation is a molasse composed of silty shale, sandstone, gravel-bearing sandstone, and conglomerate. The Amushan Formation was thought to be Carboniferous in age. However, according to the latest international stratigraphic classification standard, the upper section of the Amushan Formation is Lower Permian in age, indicating that the back-arc basin had already

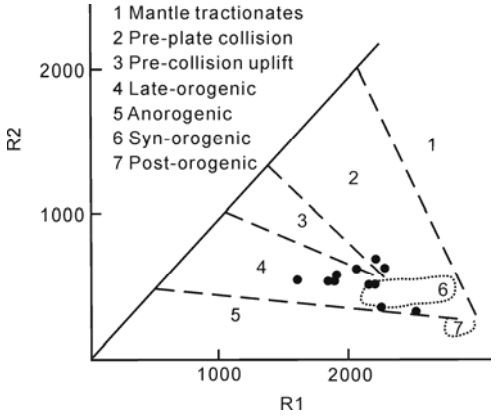

Figure 13 R1-R2 diagram [74].

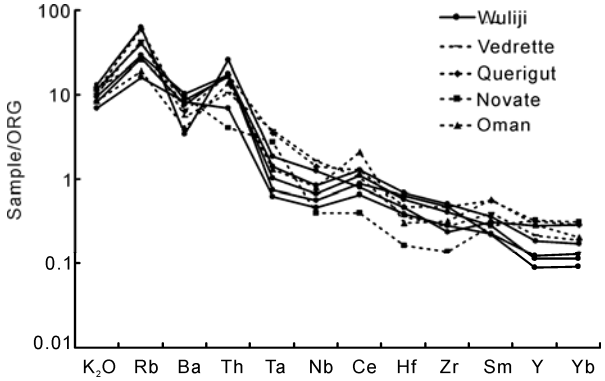

Figure 14 Ocean ridge granite (ORG) normalized geochemical patterns for samples and representative post-collision granites. The representative post-collision granites are from Vedrette di Ries, Querigut, Novate and Oman. These dates and normalized values are after ref. [50].

been closed in Early Permian. This means that the Zongnaishan-Shalazhashan Arc Zone had collided and joined with the Yabulai-Bayinnuoergong Old Continent Zone in Early Permian, and that the development of the back-arc ended and the Zongnaishan-Shalazhashan Arc Zone became accreted to the continent with arc characteristics.

The intrusive contact between the Wuliji pluton and the Amushan Formation reflects the fact that Wuliji granites formed after Late Permian. The previous lack of precise ages allowed earlier researchers to assign the Zongnaishan-Shalazhashan Zone granites to the Hercynian or Late Hercynian. The final amalgation time of the ocean represented by the Engger Us Ophiolite Belt was regarded as Late Permian or younger [18, 19, 24] or post-Permian to pre-Late Triassic [11, 12]. Presuming that Wuliji granites represent arc granites of late Permian age, the ocean represented by the Engger Us Ophiolite Belt would have still been open and the trench-arc-basin system would still have existed at that time. However, this is inconsistent with what we see in the profile of Qagan Qulu. As the source of Wuliji granites experienced the process of arc evolution, geochemical traits show arc characteristics. The values of $\varepsilon_{Nd}(t)$ also indicate the involvement of mantle-derived melt. Connecting all geochemical traits with the regional geological data, we conclude that the trench-arc-basin system really existed in Late Carboniferous in the Northern Alxa Region, and the ocean represented by the Engger Us Ophiolite Belt and the back-arc represented by the Qagan Qulu Ophiolite Belt were both closed during Early Permian, and the Northern Alxa Region entered a post-collisional period at 250.8±2.0 Ma, as indicated by Wuliji granites. This suggests that Wuliji granites are consistent with final pluton emplacement at upper crustal levels across the northern margin of the North China Plate in the Late Carboniferous to Triassic time [75–84] after melt extraction from the mantle, and ponding and underplating of this mafic material at the base of the crust.

It is difficult to determine the age of Zongnaishan-Shalazhashan Arc Zone as arc granites have not yet been recognized. According to a preliminary study of the Qagan Qulu Ophiolite Belt (unpublished data), U-Pb zircon age of gabbros is 362 Ma (only three analyses). At the same time, studies in Mongolia imply an arc-basin system also appeared north of the Engger Us Paleocean, and 325.5−332.2 Ma granites have arc characteristics, whereas 292.3 Ma granites show post-collisional characteristics [85, 86]. It may be suggested that the Carboniferous Zongnaishan-Shalazhashan Arc Zone represents only one side of a paleocean that subducted on both its margins, leading to the rapid closure of this ocean, which is also supported by the back-arc basin associated lower and middle sections of the Amushan Formation.

In conclusion, geochemical characteristics of Wuliji granites indicate that they are post-collisional granites with arc characteristics and the result of mantle-derived melt mixing with assimilated juvenile arc crust. The upper section of the Amushan Formation, which is Lower Permian in age, restricts ocean closure, represented by Engger Us Ophiolite Belt, to Early Permian. A stage of collisional orogenesis occurred after that, until about 250 Ma when the Northern Alxa Region entered into a post-collisional phase.

6 Conclusions

(1) Wuliji granites are interpreted to be post-collisional granites with arc characteristics, the result of mantle-derived melt and assimilated juvenile arc crust. The values of $\varepsilon_{Nd}(t)$ range from –0.1 to 1.3.

(2) The back-arc represented by Qagan Qulu Ophiolite Belt was closed in Early Permian. The Zongnaishan-Shalazhashan Arc Zone collided and joined with the Yabulai-Bayinnuoergong Old Continent Zone in Early Permian, and represented accreted crust of juvenile arc rocks.

(3) The Paleo-Asian Ocean represented by the Engger Us Ophiolite Belt subducted southward in Late Carboniferous time, while a trench-arc-basin system formed in the Northern Alxa Region. The Paleo-Asian Ocean was closed in Early Permian, and the Northern Alxa Region entered into a post-collisional period in Late Permian.

We thank the anonymous reviewers for their constructive reviews of this manuscript. We are grateful to Victoria Pease and Hildred Crill (Stockholm University, Sweden) for improving our English and Li Xianhua (Institute of Geology and Geophysics, Chinese Academy of Sciences) for his assistance with SIMS dating. We also thank Li Chaofeng (Institute of Geology and Geophysics, Chinese Academy of Sciences) for the help in isotopic analyses. This study was supported by National Natural Science Foundation of China (Grant No. 41040017).

1 Tang K. Tectonic development of Paleozoic fold belts at the north margin of the Sino-Korean craton. Tectonics, 1990, 9: 249–260
2 Tang K, Yan Z. Regional metamorphism and tectonic evolution of the Inner Mongolian suture zone. J Metamor Geol, 1993, 11: 511–522
3 Kheraskova T N, Didenko A N, Bush V A, et al. The Vendian-Early Paleozoic history of the continental margin of Eastern Paleogondwana, Paleoasian Ocean, and Central Asian Fold belt. Russ J Earth Sci, 2003, 5: 165–184
4 Yue Y, Liou J G, Graham S A. Tectonic correlation of Beishan and Inner Mongolia orogens and its implications for the palinspastic reconstruction of north China. In: Hendrix M S, Davis G A, eds. Paleozoic and Mesozoic Tectonic Evolution of Central and Eastern Asia: From Continental Assembly to Intracontinental Deformation. Geol Soc Am Mem, 2001, 194: 101–116
5 He G Q, Li M, Liu D Q, et al. Palaeozoic crustal evolution and mineralization in Xinjiang of China (in Chinese). Urumqi: Xinjiang People's House; Hong Kong: Educational and Cultural Press Ltd., 1994. 1–437
6 Han B F, Wang S G, Jahn B M, et al. Depleted-mantle source for the Ulungur River A-type granites from North Xinjiang, China: Geochemistry and Nd-Sr isotopic evidence, and implications for Phanerozoic crustal growth. Chem Geol, 1997, 138: 135–159
7 Wang B, Chen Y, Zhan S, et al. Primary Carboniferous and Permian

paleomagnetic results from Yili Block and their geodynamic implications on evolution of Chinese Tianshan Belt. Earth Planet Sci Lett, 2007, 263: 288–308
8 Hendrix M S, Graham S A, Amory J Y, et al. Noyon Uul Syncline, southern Mongolia: Lower Mesozoic sedimentary record of the tectonic amalgamation of Central Asia. Geol Soc Am Bull, 1996, 108: 1256–1274
9 Solomovich L I, Trifonov B A. Post-collisional granites in the South Tien Shan Variscan collisional belt, Kyrgyzstan. J Asian Earth Sci, 2002, 21: 7–21
10 Charvet J, Shu L, Laurent-Charvet S. Paleozoic structural and geodynamic evolution of eastern Tianshan (NW China): Welding of the Tarim and Junggar plates. Episodes, 2007, 30: 162–185
11 Wu T R. The composition of paleozoic lithsphere in Northern Alaxa Region and its tectonic evolution (in Chinese). Ph.D. Dissertation. Beijing: Peking University, 1990. 1–132
12 Wu T R, He G Q. Tectonic units and their fundamental chatacteristics on the northern margin of the Alxa Block. Acta Geol Sin, 1993, 6: 373–385
13 Li J Y. Permian geodynamic setting of Northeast China and adjacent regions: Closure of the Paleo-Asian Ocean and subduction of the Paleo-Pacific Plate. J Asian Earth Sci, 2006, 26: 207–224
14 Xiao W J, Windley B F, Hao J, et al. Accretion leading to collision and the Permian Solonker suture, inner Mongolia, China: Termination of the Central Asian orogenic belt. Tectonics, 2003, 22: 1069, doi: 1010.1029/2002TC1484
15 Xiao W J, Windley B F, Huang B C, et al. End-Permian to mid-Triassic termination of the accretionary processes of the southern Altaids: Implications for the geodynamic evolution, Phanerozoic continental growth, and metallogeny of Central Asia. Int J Earth Sci, 2009, 98: 1189–1217
16 Dobretsov N L, Berzin N A, Buslov M M. Opening and tectonic evolution of the Paleo-Asian Ocean. Int Geol Rev, 1995, 37: 335–360
17 Windley B F, Alexeiev D, Xiao W J, et al. Tectonic models for accretion of the Central Asian Orogenic Belt. J Geol Soc London, 2007, 164: 31–47
18 Wang T Y, Wang S Z, Wang J R. The Formation and Evolution of Paleozoic Continental Crust in Alaxa Region (in Chinese). Lanzhou: Lanzhou University Press, 1994. 1–215
19 Wang T Y, Wang J R, Wang S Z. Discover the Engger Us ophiolitic me1ange zone in North Alaxa and its tectonic significances (in Chinese). J Lanzhou Univ (Nat Sci), 1992, 28: 194–196
20 Wang J R, Song C H, Gao J P, et al. The original mechanism of the Engger Us ophiolitic mélange, North Alaxa (in Chinese). J Lanzhou Univ (Nat Sci), 1995, 31: 140–146
21 Wang T Y, Zhang M J. The characteristics and tectonics implications of the thrust belt in Eugerwusu, China (in Chinese). Sci Geol Sin, 1998, 33: 385–394
22 Wu T R, He G Q. Ophiolitic melange belts in the northern margin of the Alashan Block (in Chinese). Geosci J Graduate School China Unive Geosci, 1992, 6: 286–296
23 Wu T R, He G Q, Zhang C. On Paleozoic tectonics in the Alxa region. Acta Geol Sin, 1998, 72: 256–263
24 Wang T Y, Wang S Z. Late Paleozoic extension and tectono-magmatic evolution in the Sino-Mongolia border region in the northern part of Alxa (in Chinese). Reg Geol China, 1993, (5): 317–327
25 Wang T Y, Wang J R, Liu J K. Igneous rock associations and geochemical characteristics of volcanic arc with continental crustal basement in Zongnaishan-Shalazhashan (in Chinese). Geochimica, 1994, 23(Suppl): 62–172
26 Wang T Y, Gao J P, Wang J R, et al. Magmatism of collisional and post-orogenic period in Northern Alxa Region in Inner Mongolia (in Chinese). Acta Geol Sin, 1998, 72: 126–137
27 Zhou L R, Yu P S. The Variscan orogeny in Alxa Region (in Chinese). Northwestern Geol, 1990, (2): 22–31
28 Wang X K, Zhang L L, Liao L, et al. Geochemical characteristics and prospecting significance of the Bayannuoergong and Wuliji granite bodies in Inner Mongolia (in Chinese). Geol Miner Resour South China, 2004, (1): 24–28
29 Zhang Y Q, Han J G, Meng E G, et al. Features and tectonic significance of Saili super-unit in Bayinnuorigong area of Alashan Banner, Inner Mongolia (in Chinese). Geol Miner Resour South China, 2003, 36–40
30 Geng Y S, Wang X S, Shen Q H, et al. The discovery of Neoproterozoic Jinningian deformed granites in Alax area and its significance (in Chinese). Acta Petrol Miner, 2002, 21: 412–420
31 Ren B X, Yan G H, Mu B L, et al. Geochemistry and Nd, Sr, Pb isotopic characteristics of the alkali-rich intrusive rocks in Alxa Fault Block, Western Inner Mongolia and their implications (in Chinese). Earth Sci Front, 2005, 12: 292–301
32 Inner Mongolian Bureau of Geology and Mineral Resources. Regional Geology of Inner Mongolia (in Chinese). Beijing: Geological Publishing House, 1991. 1–725
33 Li W G, Li Q F, Jiang W D. Stratigraphy (Lithostratic) of Nei Mongol (Inner Mongolia) Autonomous Region (in Chinese). Wuhan: China University of Geosciences Press, 1996. 1–344
34 Bao Q Z, Zhang C J, Wu Z L, et al. The Carconiferous-Permian lithostratigraphic division of West Uhimqin, Inner Mongolia (in Chinese). J Stratigr, 2005, 29(Suppl): 512–519
35 Chen J F, Lu J C, Shi Z Y, et al. Development characteristics and hydrocarbon generating potential evolution of Permian-Carboniferous source rocks in Ejina Banner basin and its adjacent area, western Inner Mongolia (in Chinese), China. Geol Bull China, 2010, 29: 346–350
36 Li X H, Liu Y, Li Q L, et al. Precise determination of Phanerozoic zircon Pb/Pb age by multicollector SIMS without external standardization, Geochem Geophys Geosyst, 2009, 10: Q04010, doi: 10.1029/2009GC002400
37 Black L P, Kamo S L, Allen C M, et al. Improved $^{206}Pb/^{238}U$ microprobe geochronology by the monitoring of a trace-element-related matrix effect; SHRIMP, ID-TIMS, ELA-ICP-MS and oxygen isotope documentation for a series of zircon standards. Chem Geol, 2004, 205: 115–140
38 Wiedenbeck M, Alle P, Corfu F, et al. Three natural zircon standards for U-Th-Pb, Lu-Hf, trace-element and REE analyses. Geostand Newsl, 1995, 19: 1–23
39 Li Q L, Li X H, Liu Y, et al. Precise U-Pb and Pb-Pb dating of Phanerozoic baddeleyite by SIMS with oxygen flooding technique. J Anal At Spectrom, 2010, 25: 1107–1113
40 Stacey J S, Kramers J D. Approximation of terrestrial lead isotope evolution by a two-stage model. Earth Planet Sci Lett, 1975, 26: 207–221
41 Lugwig K R. Isoplot 3.0: A geochronological toolkit for microsoft excel. Berkeley Geochr Center Spec Publ, 2003, 4: 1–71
42 Belousova E A, Griffin W L, O'Reilly S Y, et al. Igneous zircon: Trace element composition as an indicator of source rock type. Contrib Mineral Petrol, 2002, 143: 602–622
43 Wu Y B, Zheng Y F. Genesis of zircon and its constraints on interpretation of U-Pb age (in Chinese). Chin Sci Bul1, 2004, 49: 1589–1604
44 Maniar P D, Piccoli P M. Tectonic discrimination of granitoids. Geol Soc Am Bull, 1989, 101: 635–643
45 Rickwood P C. Boundary lines within petrologic diagrams which use oxides of major and minor elements. Lithos, 1989, 22: 247–263
46 Peccerillo A, Taylor S R. Geochemistry of Eocene calc-alkaline volcanic rocks from the Kastamonu area, northern Turkey. Contrib Mineral Petrol, 1976, 58: 63–81
47 Sun S S, Mcdonough W F. Chemical and isotopic systematics of oceanic basalts: implications for mantle composition and processes. In: Saunders A D, Norry M J, eds. Magmatism in the Ocean Basins. Geol Soc Spec Publ, 1989, 42: 313–345
48 Zhang Q, Wang Y, Li C D, et al. Granite classification on the basis of Sr and Yb contents and its implications (in Chinese). Acta Petrol Sin, 2006, 22: 2249–2269
49 Zhang Q, Wang Y, Li C D, et al. A granite classification based on pressures (in Chinese). Geol Bull China, 2006, 25: 1274–1278
50 Pearce J A, Harris N B W, Tindle A G. Trace-element discrimination diagrams for the tectonic interpretation of granitic rocks. J Petrol,

1984, 25: 956–983
51 Pearce J A. Sources and settings of granitic rocks. Episodes, 1996, 19: 120–125
52 Yang Y H, Zhang H F, Chu Z Y, et al. Combined chemical separation of Lu, Hf, Rb, Sr, Sm and Nd from a single rock digest and precise and accurate isotope determinations of Lu-Hf, Rb-Sr and Sm-Nd isotope systems using Multi-collector ICP-MS and TIMS. Int J Mass Spectrom, 2010, 290: 120–126
53 Jahn B M, Wu F Y, Hong D W. Important crustal growth in the Phanerozoic: Isotopic evidence of granitoids from east-central Asia. Proc Indian Acad Sci (Earth Planet Sci), 2000, 109: 5–10
54 Jiang S H, Nie F J. Nd-isotope constrainsts on origin of granitoids in Beishan Mountain area (in Chinese). Acta Geol Sin, 2006, 80: 826–842
55 Nie F J, Jiang S H, Bai D M, et al. Metallogenic Studies and Ore Prospecting in the Conjunction Area of Inner Mongolia Autonomous Region, Gansu Province and Xinjiang Uygur Region (Beishan Mt.), Northwest China (in Chinese). Beijing: Geological Publishing House, 2002. 1–408
56 Fan H H, Min M Z, Chen J, et al. Isotopic geochemical characteristics of Yemaquan granitic intrusions in Beishan Area, Gansu Province (in Chinese). Acta Geosci Sin, 2005, 26(Suppl): 78–83
57 Hong D W, Zhang J S, Wang T, et al. Continental crustal growth and the supercontinental cycle: Evidence from the Central Asian Orogenic Belt. J Asian Earth Sci, 2004, 23: 799–813
58 Han B F, Wang S G, Jahn B M, et al. Depleted-mantle source for the Ulungur River A-type granites from North Xinjiang, China: Geochemistry and Nd-Sr isotopic evidence, and implications for Phanerozoic crustal growth. Chem Geol, 1997, 138: 135–159
59 Zhao Z H, Wang Z G, Zou T R, et al. Study on petrogenesis of alkali-rich intrusive rocks of Ulungur, Xinjiang (in Chinese). Geochimica, 1996, 25: 205–220
60 Han B F, Wang S G, Sun Y L, et al. Metalumineous-alumineous granite with positive $\varepsilon_{Nd}(T)$: Yebushan Pluton of Xinjiang. Chin Sci Bull, 1998, 43: 1323–1328
61 Wang T, Jahn B M, Kovach V P, et al. Nd-Sr isotopic mapping of the Chinese Altai and implications for continental growth in the Central Asian Orogenic Belt. Lithos, 2009, 110: 359–372
62 Zhao Z H, Wang Z G, Zou T L, et al. The REE and O, Pb, Sc and Nd compositions and the genesis types of graidtoids in Altai Mountain. In: Tu G C, ed. The Pogress of Solid Earth Science in North Xiajiang (in Chinese). Beijing: Sciences Publication House, 1993. 239–266
63 Chen B, Jahn B M, Wilde S, et al. Two contrasting paleozoic magmatic belts in northern Inner Mongolia, China: Petrogenesis and tectonic implications. Tectonophysics. 2000, 328: 157–182
64 Hong D W, Wang S G, Xie X L, et al. Genesis of positive $\varepsilon_{Nd}(t)$ granitoids in the Da Hinggan Mts.-Mongolia orogenic belt and growth continental crust (in Chinese). Earth Sci Front, 2000, 7: 441–456
65 Li H Q, Xie F C, Chang H L. Dating of Metallogenis of Metal Ore Deposits in North Xinjiang (in Chinese). Beijing: Geological Publishing House, 1998. 1–264
66 Wu F Y, Jahn B M, Wilde S, et al. Phanerozoic crustal growth: U-Pb and Sr-Nd isotopic evidence from the granites in northeastern China. Tectonophysics, 2000, 328: 89–113
67 Wu F Y, Jahn B M, Wilde S, et al. Highly fractionated I-type granites in NE China (II): Isotopic geochemistry and implications for crustal growth in the Phanerozoic. Lithos, 2003, 67: 191–204
68 Zhou T X, Chen J F, Li X M. Origin of high $\varepsilon_{Nd}(t)$ granites from Alatao Mountain, Xinjiang (in Chinese). Sci Geol Sin, 1996, 31: 71–79
69 Helo C, Hegner E, Kroner A, et al. Geochemical signature of Paleozoic accretionary complexes of the Central Asian Orogenic Belt in South Mongolia: Constraints on arc environments and crustal growth. Chem Geol, 2006, 227: 236–257
70 Jahn B M, Capdevila R, Li D Y, et al. Sources of Phanerozoic granitoids in the transect Bayanhongor-Ulaan Baatar, Mongolia: Geochemical and Nd isotopic evidence, and implications for Phanerozoic crustal growth. J Asian Earth Sci, 2004, 23: 629–653
71 Heinhorst J, Lehmann B, Ermolov P, et al. Paleozoic crustal growth and metallogeny of Central Asia: Evidence from magmatic-hydrothermal ore systems of Central Kazakhstan. Tectonophysics, 2000, 328: 69–87
72 Li C N. A geochemical method for tectonomagmatic discrimination (in Chinese). Geol Sci Technol Inf, 1992, 11: 73–78
73 Zhang Q, Wang Y L, Jin W J, et al. Criteria for the recognition of pre-, syn- and post-orogenic granitic rocks (in Chinese). Geol Bull China, 2008, 27: 1–18
74 Batchelor R A, Bowden P. Petrogenetic interpretation of granitoid rock series using multicationic parameters. Chem Geol, 1985, 48: 43–55
75 Jahn B M, Wu F Y, Chen B. Massive granitoid generation in Central Asia: Nd isotope evidence and implication for continental growth in the Phanerozoic. Episodes, 2000, 23: 82–92
76 Fan Q C, Sui J L, Liu R X, et al. Eclogite facies garnet-pyroxenolite xenolith in Hannuoba area: New evidence of magma underplating (in Chinese). Acta Petrol Sin, 2001, 17: 1–6
77 Hong D W, Huang H Z, Xiao Y J, et al. The Permian alkaline granites in central Inner Mongolia and their geodynamic significance (in Chinese). Acta Geol Sin, 1994, 68: 219–230
78 Shao J A, Zhang R H, Han Q J, et al. Geochronology of cumulate xenoliths and their host diorites from Harqin, eastern Nei Mongol (in Chinese). Geochimica, 2000, 29: 331–336
79 Shao J A, Han Q J, Zhang L Q, et al. Found of the xenoliths from Early Meszoic accumulational complex in the eastern Inner Mongolia. Chin Sci Bull, 1999, 44: 478–485
80 She H Q, Xu G Z, Zhou R, et al. Tectonic and magmatic activities in early Mesozoic and their controlling on gold mineralization in Honghuagou gold ore field, Inner Mongolia (in Chinese). Geoscience, 2000, 14: 408–416
81 She H Q, Wang Y W, Li Q H, et al. The mafic granulite xenoliths and its implications to mineralization in Chaihulanzi Gold Deposit, Inner Mongolian, China (in Chinese). Acta Geol Sin, 2006, 80: 863–875
82 Zhang X H, Zhang H F, Tang Y J, et al. Early Triassic A-type felsic volcanism in the Xilinhaote-Xiwuqi,central Inner Mongolia: Age, geochemistry and tectonic implications (in Chinese). Acta Petrol Sin, 2006, 22: 2769–2780
83 Shi G H, Miao L C, Zhang F Q, et al. Emplacement age and tectonic implications of the Xilinhot A-type granite in Inner Mongolia, China. Chin Sci Bull, 2004, 49: 723–729
84 Zhang X H, Zhang H F, Zhai M G, et al. Geochemistry of Middle Triassic gabbros from northern Liaoning, North China: Origin and tectonic implications. Geol Maga, 2009, 146: 540–551
85 Batkhishig B, Noriyoshi T, Greg B. Magmatism of the Shuteen Complex and Carboniferous subduction of the Gurvansaikhan terrane, South Mongolia. J Asian Earth Sci, 2010, 37: 399–411
86 Blight J H S, Crowley Q G, Petterson M G, et al. Granites of the Southern Mongolia Carboniferous Arc: New geochronological and geochemical constraints. Lithos, 2010, 116: 35–52